IIETA International Information and Engineering Technology Association
Advancing the World of Information and Engineering

Instrumentation Mesure Métrologie
Vol. 23, No. 3, June, 2024, pp. 193-198
Journal homepage: http://iieta.org/journals/i2m

Numerical Modeling and Analysis of the Pressure Pulse Generated by Drop Mass Calibration Device

Ahmed H. Mokhtar[1*], Ragaie M. Rashad[1], T. A. Osman[1], Alaaeldin A. Eltawil[2], Shaker A. Gelany[2]

[1] Mechanical Design and Production Engineering Department, Cairo University, Giza 12613, Egypt
[2] Mass, Density and Pressure Laboratory, National Institute of Standards, Giza 12211, Egypt

Corresponding Author Email: ahmed.hamed@cu.edu.eg

https://doi.org/10.18280/i2m.230302

Received: 4 April 2024
Revised: 2 June 2024
Accepted: 13 June 2024
Available online: 21 June 2024

Keywords:
bulk modulus, calibration, dynamic pressure, drop mass device, effective bulk modulus

ABSTRACT

This study focuses on the development of a computational fluid dynamics (CFD) model using Ansys Fluent to predict maximum pressure and pressure changes over time. The accuracy of hydraulic modeling is directly influenced by the bulk modulus of hydraulic oil, making it a crucial characteristic to study. Experimental data was used to validate the results obtained from the CFD model. Furthermore, an in-depth investigation was conducted to analyze the fluid bulk modulus and its correlation with the presence of air trapped inside the cylinder. The findings of this research provide valuable insights into the behavior of hydraulic systems and the importance of accurate fluid property characterization for effective modeling.

1. INTRODUCTION

The limitations of static pressure sensors for capturing dynamic pressure changes became evident in the 1960s, sparking a surge of interest in sensors capable of capturing non-stationary pressure variations and the methods to calibrate them. This newfound attention stemmed from industries like aerospace and military, where reliable pressure measurements are critical. Programs involving missiles and space vehicles, as Schweppe et al. [1] noted, demanded accurate solutions for rapidly changing pressure signals. This need resonated across other fields as well; Eichstädt [2] highlighted the automotive industry's reliance on sensors that could track dramatic and rapid pressure fluctuations. Hjelmgren [3] further emphasized the importance of dynamic pressure measurements in diverse areas like medicine and robotics.

Recognizing the need for standardization, the American Society of Mechanical Engineers (ASME) published a landmark guide in 1972 titled "Guide to Calibrating Pressure Transducers." This document, mentioned as the gold standard in dynamic pressure transducer calibration, was later reissued by the Instrumentation Systems and Automation Society (ISA) in 2002 [4]. The guide delves into crucial aspects of dynamic calibration, including the behavior of pressure transducers in the frequency and time domains, mathematical models employed for calibration, specific calibration devices, and considerations for optimizing the electronics involved. Notably, it does not address methods for estimating uncertainties associated with pressure transducer measurements.

The field of dynamic pressure sensor calibration continues to evolve, attracting active research from established institutions like the National Physical Laboratory (NPL) in England and the Physikalisch-Technischen Bundesanstalt (PTB) in Germany. Additionally, large corporations like Rolls-Royce, Volkswagen, and Porsche are invested in improving dynamic pressure measurement processes due to its relevance to their operations [5].

The bulk modulus is a crucial parameter in fluid power applications and is commonly described as the inverse of compressibility [6]. It indicates the system's rigidity and the speed at which pressure waves propagate. Consequently, the stability of servo-hydraulic systems and the efficiency of hydraulic systems are significantly influenced by the fluid's bulk modulus. Hence, understanding the accurate bulk modulus of hydraulic fluids and the various factors that impact its numerical value is of utmost importance [3].

Kneževic et al. [7] provided a diagram that shows how the bulk modulus changes with respect to both temperature and pressure. The data's validity was indirectly verified by comparing it to experimental measurements of pressure changes during the decompression of mineral oil within hydraulic cylinders. A similar model was developed in this paper; however, the temperature was kept constant throughout the experiment and the model.

According to Henry's Law, the amount of gas dissolved in a liquid increase with the pressure of the gas, as long as the temperature remains constant. This law describes how gases dissolve in various liquids, including oil. The capacity of a liquid to dissolve gas is termed its solubility [8]. The presence of entrained air in hydraulic oil can lead to several negative consequences [9]: (1) Increased compressibility: as air is much more compressible than oil; (2) Higher viscosity: air bubbles can disrupt the flow of oil, increasing its overall resistance to

movement (viscosity); (3) Liquid breakdown: Entrained air can promote cavitation, a phenomenon where bubbles form, collapse rapidly, and create localized shockwaves that can damage the oil and surrounding components; (4) Reduced heat conductivity: Air is a poor conductor of heat compared to oil. Entrained air bubbles can impede the oil's ability to transfer heat away from critical components, potentially leading to overheating issues.

This study focused on the development of a numerical CFD model to reliably evaluate pressure waves inside a piston cylinder chamber to perform dynamic pressure calibration for the establishment of a traceable dynamic calibration method for high-pressure sensors. Also to evaluate the effective fluid bulk modulus and the relation between bulk modulus and entrapped air inside the cylinder.

2. EXPERIMENTAL SETUP

The experimental work has been carried out at National Institute of Standards (NIS) in Egypt. The main goal of the experiment is to calibrate a dynamic pressure transducer against a standard one. Gelany [10] proposed a system that generates dynamic pressure through a simple yet effective process. A free-falling mass, guided by a precise system, impacts a piston within a hydraulic cylinder, as shown in Figure 1. This impact compresses the oil, creating a dynamic pressure pulse [11]. As the kinetic energy of the falling mass converts to the oil's elastic energy, the piston reaches its maximum compression and the pressure peaks [12]. The oil's natural elasticity then pushes the piston back up, ejecting the mass and transforming the stored energy back into the mass's potential energy. Figure 2 shows the setup components. The result is a roughly half-sine pressure pulse within the cylinder. The aim was to provide traceability to dynamic pressure sensors and transducers using the falling mass method.

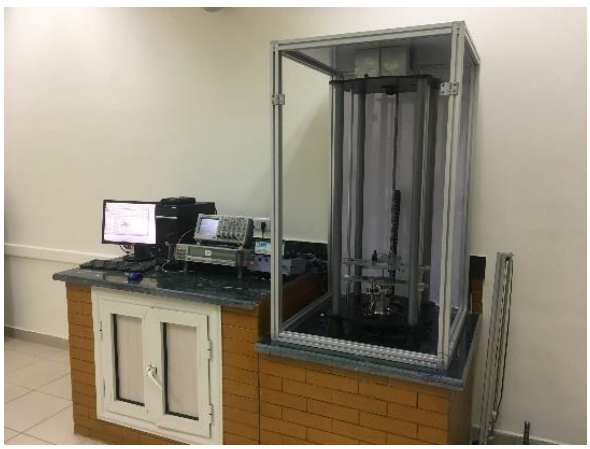

Figure 1. Setup overview

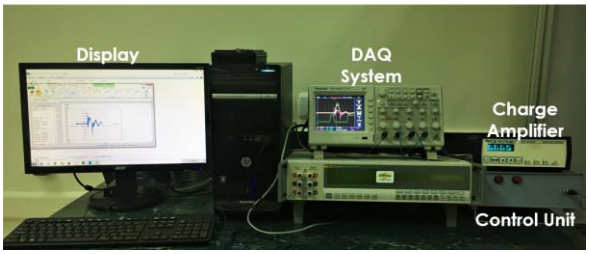

Figure 2. Setup components

2.1 Pressure cell

The pressure cavity is completely filled with a fluid transmitting medium. After the piston was hit by the falling mass, it compresses oil inside the cavity. The pressure is then transmitted to both the standard and the calibrated sensors. Figure 3 shows pressure cell parts.

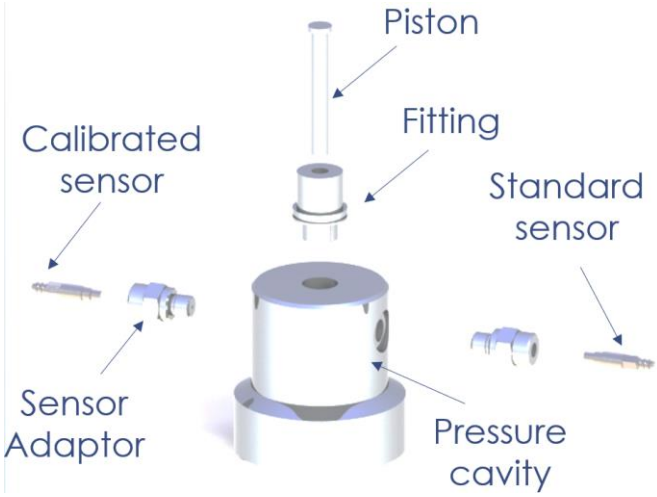

Figure 3. Pressure cell exploded view

3. THE NUMERICAL MODEL

The numerical model of the pressure pulse generated was developed with Ansys Fluent. Since this experiment involves a fluid medium contained inside a rigid/undeformed structure, the fluid medium was modeled as 2D axisymmetric about the x axis. Although the domain is not totally axisymmetric and the results will have some faults due to the narrow channels where the pressure sensors were fitted, the two dimensions have the advantage of being computationally smoother than building a full 3D model, while also permitting for simpler application of boundary conditions and simpler meshing.

The fluid used in the experiment is Di(2-EthylHexyl) Sebacate (DEHS). DEHS, a diester with 96% biodegradability, is synthesized from a linear diacid and a monofunctional alcohol. Its fundamental application lies in its role as a Pressure Transfer Fluid (PTF) within various hydraulic systems. These systems include; hydraulic pressure balances, pressure measuring instruments, internal combustion engines, processing equipment, hydraulic pumps and compressors, gears and final drives. Furthermore, the viscoelastic properties (combined viscous and elastic behavior) of DEHS are a critical factor considered during the design of high-pressure piston standards [13]. It is also a key factor to account for when representing metrologically the piston gauge. DEHS is a valuable industrial reference fluid in the field of applications with = moderately high viscosity and high pressures [14]. Di(2-EthylHexyl) Sebacate is also used in boundary lubricating applications. This fluid's resistance to oxidation, low volatility, and high flash point makes it a suitable candidate for use as both an oil additive and a base oil [15].

Oil properties at 38°C [14, 16]
Density (ρ) = 913.8 kg/m^3
Viscosity (η) = 21.14 mPa.s
Isothermal Bulk Modulus = 1.35 GPa

3.1 Meshing

Since the mesh cells of a compressing fluid domain is a deforming mesh, the dynamic mesh model was chosen. The dynamic mesh model in computational fluid dynamics allows for boundaries within a cell zone to move and deform. This enables the mesh to adapt to these changes, ensuring accurate simulations. These boundaries can undergo rigid motion or deformation. Rigid motion includes linear movements (translation) or rotations relative to each other while deformation the boundaries themselves can stretch, bend, or compress during the simulation. This flexibility allows for simulating scenarios with complex moving parts or fluid-structure interactions [17].

Knowing the fact that the fluid domain was modeled as 2D quadrilateral, the dynamic layering technique was used. This technique dynamically adjusts the mesh near moving boundaries. It achieves this by adding or removing layers of cells based on the distance (height) between the closest cell layer and the moving surface.

In Ansys Fluent's dynamic mesh model, users can define a target cell size (ideal layer height) for each moving boundary. The software then manages the cells adjacent to the boundary (layer j in Figure 4). If these cells (layer j) become too large or small compared to the target size, Fluent will either split or merge the layer. Splitting divides layer j into smaller cells to maintain the desired resolution near the moving boundary, while merging the layer combines layer j with its neighbor (layer i) if the cells in j become too small, improving computational efficiency [17].

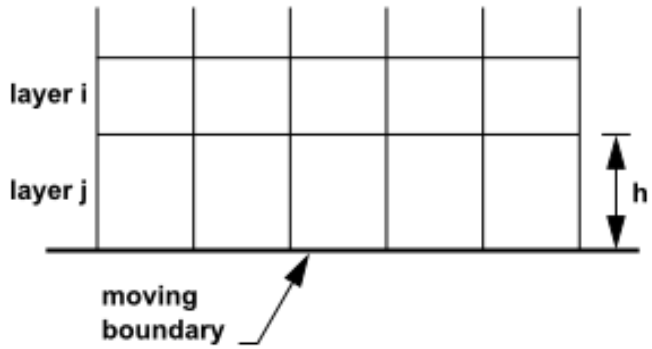

Figure 4. Dynamic layering

If the cells in layer j are expanding, the cell heights are allowed to increase until

$$h_{min} > (1 + \alpha_s)\, h_{ideal} \qquad (1)$$

where, h_{min} is the minimum cell height of cell layer j, h_{ideal} is the ideal cell height and should be defined by the user, and α_s is the layer split factor. When the condition in Eq. (1) is satisfied, indicating a need for mesh refinement, Ansys Fluent provides two options for splitting the cells adjacent to the moving boundary. These options are height-based layering, which refines the mesh based on a specified constant target cell height h_{ideal} near the boundary, or ratio-based layering, which controls, locally, the ratio α_s between the size of the cell adjacent to the boundary and the size of its neighboring cells.

In the case of compressing layer j (as in the applications of compressing oil), they can be compressed until Eq. (2) is met.

$$h_{min} < \alpha_c\, h_{ideal} \qquad (2)$$

where, α_c is the layer collapse factor. When the software detects the satisfaction of this condition, Ansys Fluent takes action to optimize the mesh. It achieves this by merging the compressed cell layer, denoted as Layer j in Figure 4, with the layer directly above it (layer i). In other words, the software combines the cells in these two layers to improve computational efficiency.

3.2 Grid generation

Since the computational fluid domain of the piston is axisymmetric, one half of the domain is shown in Figure 5. It is comprised of cylinder walls (left and upper walls) and piston head (right wall). The piston wall behaves as the moving boundary. A clearance film above the piston walls of size 0.184 mm is meshed differently from the rest of the mesh domain. The clearance zone was finely meshed relative to other domain to obtain the highest possible accuracy when measuring the induced pressure inside the cylinder. However the grid is not changing in size along the x axis.

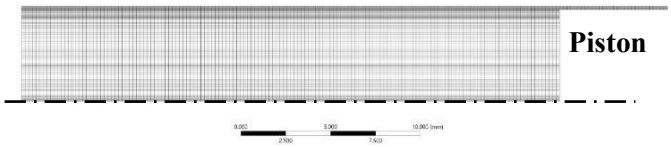

Figure 5. Generated grid inside the cylinder

3.3 Boundary conditions

The simulation is initialized at atmospheric pressure taking the gravity effect into consideration. The data from the velocity sensor measuring contact velocity when the falling mass immediately hitting the piston is fitted to a polynomial equation. The fitted equation was compiled to the CFD solver using the User Defined Function UDF [18]. Figure 6 shows the measured values from the sensor versus the fitted polynomial showing that there is almost no noticeable error. Also, Figure 6 shows the rebound velocity of the mass and the piston after compression.

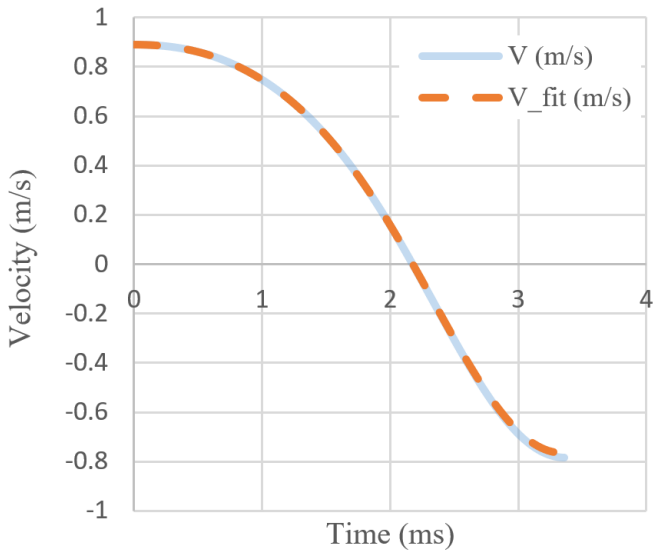

Figure 6. Measured vs fitted velocities

4. RESULTS AND DISCUSSIONS

The experiment was conducted at 3 different levels. Table 1 summarizes the key findings regarding the maximum piston displacement and cylinder pressure. The displacement was measured using numerical integration for the results from the accelerometer attached to the falling mass. The maximum pressure data was collected from the piezoelectric transducers fitted to the cylinder. As the maximum pressure can be predicted theoretically [19], Eq. (3) has been used to predict effective bulk modulus at each height (Table 1). It assumes that a mass M falls from a height h to strike the piston cylinder. The cylinder has area A, and the initial volume inside the cylinder is V_0 . The key parameters of the drop-mass calibration device setting are as follows: M = 4.34 kg, V_0 = 2.64 cm^3, A = 0.81 cm^2, local gravity g = 9.793 m/s^2 and the sebacate oil used as the hydraulic oil K_0 =1350 MPa.

The results reveal a significant difference between the effective bulk modulus measured in the experiment and the theoretical isothermal tangent bulk modulus of sebacate without air. The effective bulk modulus is nearly 60% lower, highlighting the substantial influence of even a small amount of entrapped air within the cylinder. To account for this real-world effect, the model adopted the experimentally determined effective bulk modulus rather than the theoretical absolute value. Undissolved gas bubbles can significantly alter a liquid's properties and how it responds to mechanical stresses [20].

$$K_e = \frac{{P_{max}}^2 V_0}{2Mgh} \tag{3}$$

Table 1. Experimental results at different heights

h (cm)	x_{max} (mm)	P_{max} Exp. (Mpa)	K_e (MPa)
5	1.36	30.20	567.14
7	1.86	35.32	554.04
10	2.64	41.03	523.45

Fitting data in Table 1 with the power function, we get

$$P_{max} = 14.867\, h^{0.442} \tag{4}$$

where, the power exponent h is less than 0.5, according to Eq. 3, the prediction P_{max} should be proportion to $\sqrt{h}$. Eq. (3) incorporates parameters like mass (M) and initial oil volume (V_0). These represent inherent properties of the drop-mass calibration device and are constant, independent of the drop height (h). This implies that the bulk modulus, as represented in the equation, solely reflects the influence of the initial drop height (h). However, there's a crucial aspect to consider: the initial height (h) is directly related to the relative compression experienced by the oil ($\Delta V/V$).

To account for this relationship, a more accurate representation of the hydraulic oil's behavior is necessary. We should consider a model that reflects a fluid spring with variable stiffness. This model acknowledges that the stiffness of the oil changes progressively as it undergoes compression during the impact process.

This revised model aligns with the observed phenomenon. As the initial drop height (h) increases, the oil experiences greater compression. Consequently, the effective stiffness of the oil increases. This explains why the observed pressure peak is lower than anticipated when the initial drop height is increased. The oil's stiffness absorbs a portion of the impact energy, resulting in a lower peak pressure compared to a scenario with constant stiffness. Some existing models like the presented by Fei et al., present a higher value for height power exponent [19].

Figure 7 shows the pressure pulse induced in the cylinder after being hit by the falling mass. At 5 cm falling height, the maximum pressure (MPa) from the transducer fitted to the cylinder and the CFD model are 30.20 and 29.34 respectively. The variation between experimental and numerical results is highly visible at the start and end of the curve. As a result of entrapped air existence inside the cylinder, the slope at the beginning of the curve is not constant. On the other hand, the model was built as the piston chamber completely filled with oil, so the effective bulk modulus of the oil is the only affecting the pressure pulse generated.

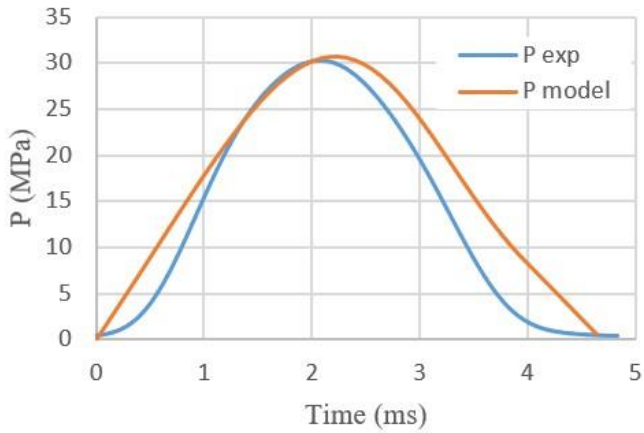

Figure 1. Experimental vs analytical results for pressure with time

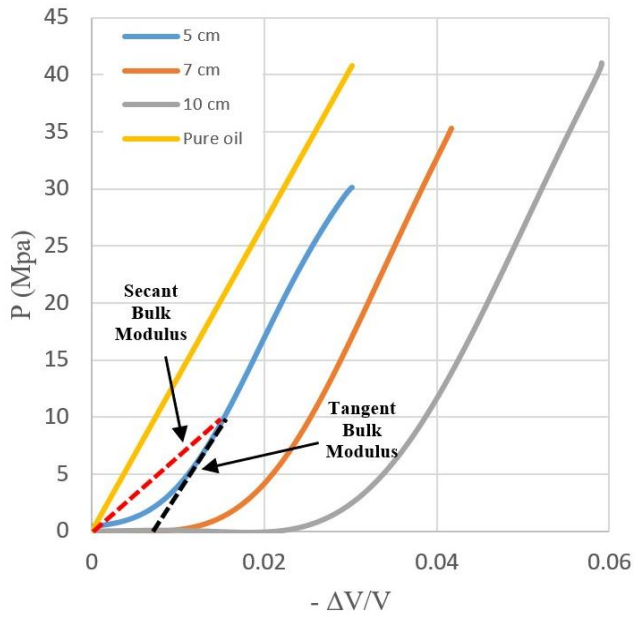

Figure 2. Pressure vs relative change in volume of the oil at different dropping heights

In order to experimentally investigate the oil bulk modulus, the pressure induced was recorded versus the change in volume per volume at different falling heights. The slope of each curve on the chart (Figure 8) should be the isothermal tangent bulk modulus of the oil filling the cylinder (1350 MPa).

The straight line passing through the origin is for the pure oil with zero air percentage. Every time the experiment was conducted at a specific height, the slope of the line at low pressure decreases. Figure 8 highlights a key observation which is the secant bulk modulus of the mixture deviates from the tangent bulk modulus (considered the true bulk modulus) at lower pressure regions. This difference suggests that using the tangent bulk modulus definition might be more appropriate for analyzing the material's behavior in this pressure range.

5. CONCLUSIONS

In this paper, a numerical model was proposed for the fluid inside the cylinder in a drop mass experiment. Experimental data were used to validate the results from the model. Fluid bulk modulus was analyzed using experimental data. As a result of the entrained air, the magnitude of the bulk modulus drastically reduced compared to pure oil.

An empirical formula was introduced to relate the maximum pressure inside the cylinder and the falling height. This mathematical description should be very helpful when studying the dynamic behavior of hydraulic actuators. While the temperature was kept constant throughout the experiment, the future work intends to study the change of fluid bulk modulus with both pressure and temperature.

This limitation of 2D analysis can significantly affect the generalizability of the CFD results. Since the model doesn't account for 3D effects, the findings might not be directly applicable to situations involving even minor geometric variations or complexities. For instance, the 2D model wouldn't capture the formation of drag-inducing vortices behind the cylinder, potentially underestimating the actual impact force experienced. Therefore, it's crucial to carefully consider the potential impact of 2D limitations when interpreting and applying the results to real-world scenarios with even slight 3D characteristics. This will be the scope of the future research.

REFERENCES

[1] Schweppe, J.L., Eichberger, L.C., Muster, D.F., Michaels, E.L., Paskusz, G.F. (1963). Methods for the Dynamic Calibration of Pressure Transducers. US Department of Commerce, National Bureau of Standards Monograph 67.

[2] Eichstädt, S. (2012). Analysis of dynamic measurements: Evaluation of dynamic measurement uncertainty. Wirtschaftsverl. NW, Verlag für Neue Wiss.

[3] Hjelmgren, J. (2002). Dynamic measurement of pressure-A literature survey. SP Technical Research Institute of Sweden.

[4] American Society of Mechanical Engineers. (1972). A Guide for the Dynamic Calibration of Pressure Transducers. ASME.

[5] EMRP. (2015). Industrial dynamic measurements: A best practice guide dynamic pressure. Traceable Dynamic Measurement of Mechanical Quantities. https://www.ptb.de/emrp/2175.html.

[6] Manring, N.D., Fales, R.C. (2019). Hydraulic Control Systems. John Wiley & Sons.

[7] Kneževic, D., Milašinovic, A., Milovanovic, Z., Savic, V. (2011). Analysis of changes of bulk modulus of mineral oil—Effects on the dynamic behavior of hydraulic actuators. In 12th International Conference on Tribology—Serbiatrib'11, Kragujevac, Serbia, pp. 370-375.

[8] Totten, G.E., De Negri, V.J. (2011). Handbook of Hydraulic Fluid Technology. CRC press.

[9] Kiani-Oshtorjani, M., Mikkola, A., Jalali, P. (2023). Novel bulk modulus model to estimate stiffness in fluid power systems. Mechatronics, 92: 102987. https://doi.org/10.1016/j.mechatronics.2023.102987

[10] Gelany, S. (2019). Establishment and characterization of reference system for calibration of dynamic pressure sensors. Faculty of Engineering, Cairo University.

[11] Salminen, J., Högström, R., Saxholm, S., Lakka, A., Riski, K., Heinonen, M. (2018). Development of a primary standard for dynamic pressure based on drop weight method covering a range of 10 MPa–400 MPa. Metrologia, 55(2): S52. https://doi.org/10.1088/1681-7575/aaa847

[12] Bruns, T., Franke, E., Kobusch, M. (2013). Linking dynamic to static pressure by laser interferometry. Metrologia, 50(6): 580. https://doi.org/10.1088/0026-1394/50/6/580

[13] Sahin-Dinc, F. (2023). Dynamic viscosity of some lubricants in terms of local nano-void fraction. Acta Physica Polonica: A, 144(3): 180-196. http://doi.org/10.12693/APhysPolA.144.180

[14] Paredes, X., Fandiño, O., Pensado, A.S., Comuñas, M.J., Fernández, J. (2012). Experimental density and viscosity measurements of di (2ethylhexyl) sebacate at high pressure. The Journal of Chemical Thermodynamics, 44(1): 38-43. https://doi.org/10.1016/j.jct.2011.07.005

[15] Boiko, M.V., Sidashov, A.V., Boiko, T.G., Burykin, I.V., Uflyand, I.E. (2022). The mechanism of formation of boundary lubricating films during friction in a medium of di (2-ethylhexyl) sebacate. Tribology International, 165: 107222. https://doi.org/10.1016/j.triboint.2021.107222

[16] Mylona, S.K., Assael, M.J., Antoniadis, K.D., Polymatidou, S.K., Karagiannidis, L. (2013). Measurements of the viscosity of bis (2-ethylhexyl) sebacate, squalane, and bis (2-ethylhexyl) phthalate between (283 and 363) K at 0.1 Mpa. Journal of Chemical & Engineering Data, 58(10): 2805-2808. https://doi.org/10.1021/je4005245

[17] Ansys Help (2024). https://ansyshelp.ansys.com.

[18] ANSYS Inc. (2000). ANSYS FLUENT UDF Manual. Canonsburg, PA, pp. 724–746.

[19] Fei, S., Kong, D. (2011). Bulk modulus measurement of hydraulic oil based on drop-hammer calibration device. In 2011 International Conference on Electric Information and Control Engineering, Wuhan, China, pp. 213-216. https://doi.org/10.1109/ICEICE.2011.5778375

[20] Troyakov, K.V., Kaverzina, A.S., Rybin, V.V., Ivanov, A.Y., Kardash, A.A. (2024). Effect of undissolved gas on fluid bulk modulus. E3S Web of Conferences, 471: 02019. https://doi.org/10.1051/e3sconf/202447102019

NOMENCLATURE

A	area, m^2
g	gravitational acceleration, $m.s^{-2}$
h	falling height, m
K	bulk modulus, Pa
M	mass, kg
p	pressure, Pa
V	volume, m^3
x	piston displacement, m

Greek symbols

α	layer factor
ρ	fluid density, $kg.m^{-3}$
η	fluid viscosity Pa.s

Subscripts

c	collapse
e	effective
exp	experimental
f	fluid
s	split